Scientific Research Publishing

Litho-Tectonic Architecture of the Dialafara Area, Kédougou-Kéniéba Inlier, Integration of New Field Data and Geophysics

Mahamadou Diallo[1]* , Mamadou Yossi[2], Ibrahim Méyès Coulibaly[1], Youssouf Son[1], Amako Dolo[1]

[1]Département de Géologie et Mines, Ecole Nationale d'Ingénieurs Abderhamane Baba Touré (ENI-ABT), Bamako, Mali
[2]Sagax Afrique S.A Geophysical Surveys and Consulting, Bamako, Mali
Email: *mahamadou.diallo@mesrs.ml, *yaranga.mdiallo@gmail.com

Abstract

The Dialafara area is part of the highly endowed Kédougou-Kéniéba Inlier (KKI), West-Malian gold belt, which corresponds to a Paleoproterozoic window through the West African Craton (WAC). This study presents, first of all, an integration of geophysical data interpretation with litho-structural field reconnaissance and then proposes a new litho-structural map of the Dialafara area. The Dialafara area shows a variety of lithology characterized by volcanic and volcano-sedimentary units, metasediments and plutonic intrusion. These lithologies were affected by a complex superposition of structures of unequal importance defining three deformation phases (D_{D1} to D_{D3}) under ductile to brittle regimes. These features permit to portray a new litho-structural map, which shows that the Dialafara area presents a more complex lithological and structural context than the one presented in regional map of the KKI. This leads to the evidence that this area could be a potential site for exploration as it is situated between two world-class gold districts.

Keywords

Kédougou-Kéniéba Inlier, Dialafara, Mapping, Aeromagnetic Data, Structure

1. Introduction

Several studies have explained the evolution of Precambrian terranes with a complex tectonic history and a wide potential in mineral resources (especially in gold; [1]). Paleoproterozoic terranes of the Man-Leo Rise in the southern part of the West African Craton (WAC; **Figure 1**) were deformed and metamorphosed during the Eburnean orogeny dated between ca. 2250 and 1980 Ma [2] [3] [4] [5].
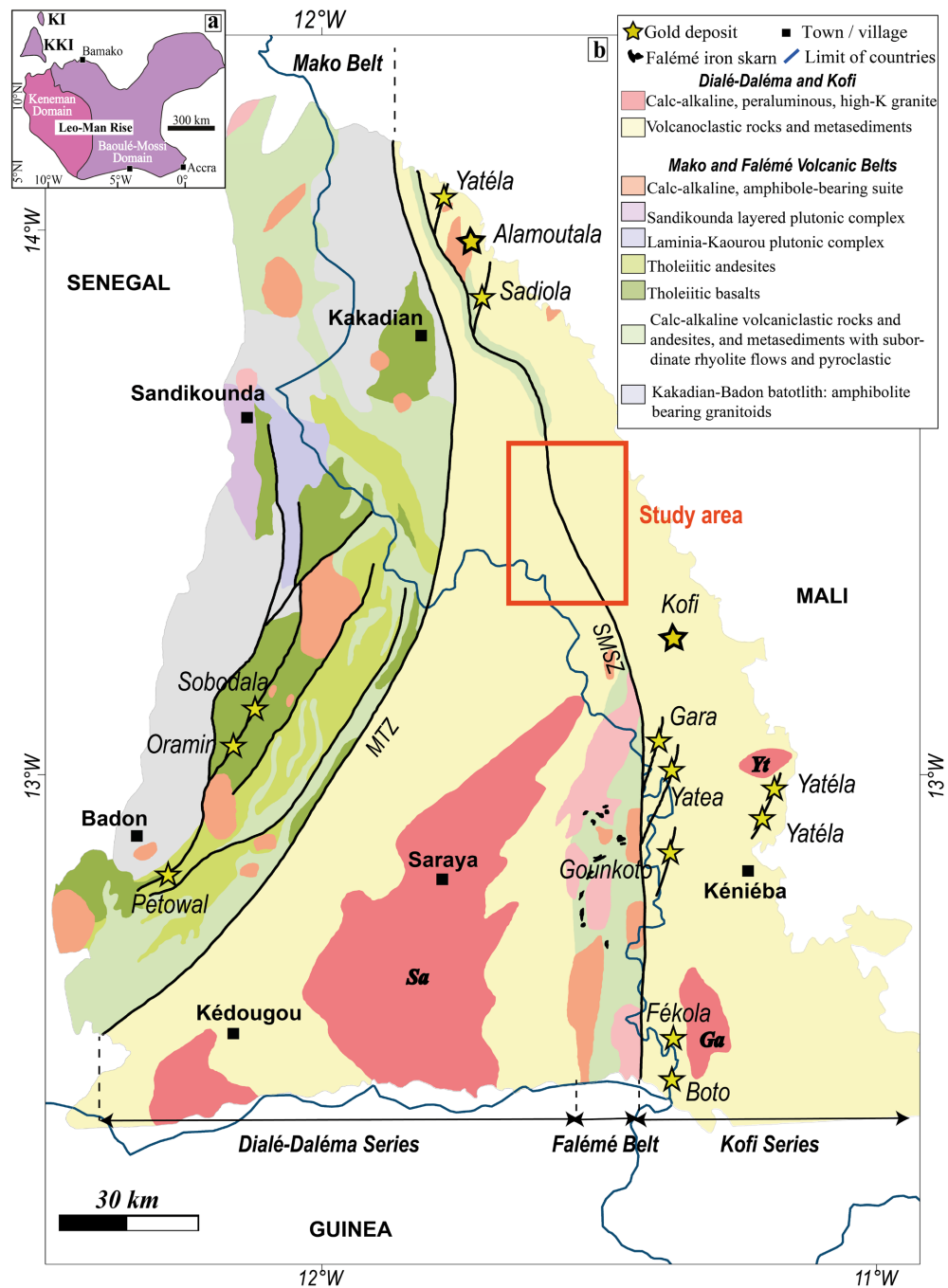
Figure 1. (a) Simplified geological map of the Leo-Man Shield. (b) Geologic map of the Paleoproterozoic Kédougou-Kéniéba inlier (modified after Gueye *et al.*, 2008; Masurel *et al.*, 2017c). Abbreviations: Ga: Gamaye monzogranite; KI: Kayes Inlier; KKI: Kédougou-Kéniéba Inlier; Sa: Saraya pluton; Yt: Yatea monzogranite.

Eburnean orogeny is an important period of crustal thickening during the Proterozoic and there are still gaps in the design of the processes involved (e.g., [6] [7]). This orogenic evolution is generally marked by a diversified range of magmatism in different tectonic contexts (e.g., [8]) and developed a distinct metallogenic province [9] [10].

Concerning questions about the deformation style of the Paleoproterozoic formations of the WAC, the Kédougou-Kéniéba Inlier (KKI) occupies a special place because of its isolated position in the center-west of the craton (**Figure 1**) and represents one of the most perspective regions for gold and other mineralization in West Africa (e.g., [1] [11]). The KKI is the northern part of the Baoulé-Mossi domain and shares with it a same litho-tectonic context (e.g., [12]). The deciphering of the litho-tectonic context of these formations improves our understanding of the evolution of this part of the Craton.

Outcrop conditions are poor in the KKI, requiring the contribution of other techniques to characterize the litho-tectonic context such as geophysics. Aeromagnetic data provides better resolution of near-surface and can be used to identify lithological units, faults, and their prolongation as major crustal shear zones [13] [14]. Statistical analysis of K, U and Th concentrations of airborne gamma-ray spectrometric data and its qualitative analysis of the RGB ternary composition image can contribute significantly to elaborate a litho-tectonic map of a region (e.g., [15] [16]).

The most gold production of the KKI is mainly articulated around the deposits located within the Kofi series in Mali (**Figure 1**). These deposits are: 1) Sadiola, Alamoutala and Yatela (Sadiola district) in the northern end of the Kofi series, 2) Gara, Yaléa, Gounkoto forming the Loulo district within the middle part of the series with the deposits of Tabakoto and Ségala further east, and finally 3) Fékola to the south of the Kofi series (**Figure 1**). The Dialafara zone is situated between the Sadiola district in the north and the Loulo district in the south (**Figure 1(b)**).

To complement the understanding of the Paleoproterozoic KKI and to fill gaps between the Sadiola and Loulo districts, this paper presents an integration of original field work and analysis of airborne magnetic and gamma-ray spectrometric data of the Dialafara zone. We aim to determine the main litho-structural frameworks of the area and possible mineralized structures as an attempt to foment new information for further prospective campaigns.

2. Geological Setting

The Kédougou-Kéniéba Inlier (KKI) is made of Paleoproterozoic rocks deformed and metamorphosed during the Eburnean orogeny [2]. The KKI is made by two metavolcanic belts (Mako and Falémé belts) and two metasedimentary series (Dialé-Daléma and Kofi series) [17] (**Figure 1(b)**).

The Mako belt (**Figure 1(b)**) is composed of basaltic (locally displaying pillow lavas), gabbroic and ultramafic rocks of tholeiitic affinity as well as intermediate to dacitic volcanic and volcaniclastic rocks [18] [19]). The Mako belt is also intruded by the Kakadian batholith and numerous small granitoid plutons [8] [17]. The Falémé belt (**Figure 1(b)**) is made by metamorphosed volcanic sequence (andesite flows with preserved pillowed structures, subordinate rhyodacite lavas and pyroclastic rocks) interbedded with metasedimentary rocks (me-

tavolcanoclastics, metagreywackes and metacarbonates) and syntectonic granitoid plutons [17] [20] [21]. Plutonic intrusions are represented by the Balangouma, Falémé Sud and Boboti plutons [17] [22]. The Dialé-Daléma and Kofi metasedimentary series (**Figure 1(b)**) are derived from erosion of the Mako belt [23] [24]. These series are composed by a wide range of siliciclastic and impure carbonate rocks [17] [20]. The metasedimentary rocks are intercalated with volcaniclastic rocks and rhyolite flows [17] [20]. The Dialé-Daléma and Kofi series are intruded by numerous syntectonic granitoid plutons [8] [25] [26] [27] such as Saraya batholith, Gamaye pluton and Yatea pluton.

In most regions of the craton, Eburnean orogeny is characterized by a polycyclic evolution [12]. In the KKI, previous work distinguishes three major phases of Eburnean deformation starting by an early period of shortening (D_1) which is followed by a period of transcurrent tectonics (D_2-D_3) (e.g., [8] [26] [27] [28] [29] [30]). The D_1 phase is marked by crustal thickening, which is associated with SE verging thrusts and stratigraphic stacking with associated folding, prior to widespread granitoid plutonism throughout the KKI [8] [28] [29]. However, little is known about the kinematics of the D_1 due to penetrative reworking by subsequent deformation. The D_2 and D_3 transcurrent phases structures mark the main tectonic footprints of the KKI during which folding was followed by sinistral displacement on north-striking shear zones [12] [28] [30] [31]. These phases are associated with the widespread granitoid plutonism throughout the KKI [8] [17]. Two main regional shear zones were described during the D_2-D_3 transcurent phases in the KKI: 1) The Main Transcurrent Zone (MTZ) [28], which separate the metavolcanic belts of Mako from the metasedimentary Dialé-Daléma series and 2) the Senegalo-Malian Shear Zone (SMSZ) [31], which separates the Faléme belt from the Kofi series in the south and, further north, the Dialé-Dalema from the Kofi series.

3. Methodology and Data Use

The approach in this paper is to combine different information in an integrated dataset in a complementary manner. These data are the litho-structural features from field work and the interpretation of geophysical data. The flowchart of the main research steps followed during this paper is illustrated in **Figure 2**.

3.1. Field Work

Field work was made to constrain the lithological and structural context of the study area. However, traverses were designed prior to the field work based on the literature review. Thus, the methodology used in this study was the transect mapping: several cross-sections were made on foot following a predefined direction. However, data were also collected during road traverse (**Figure 3**). During field work, the identification and description of structures were collected in conjunction with lithological and petrographic data from the study area during the various traverses. This work allows establishing an outcrop database (**Figure 3**)
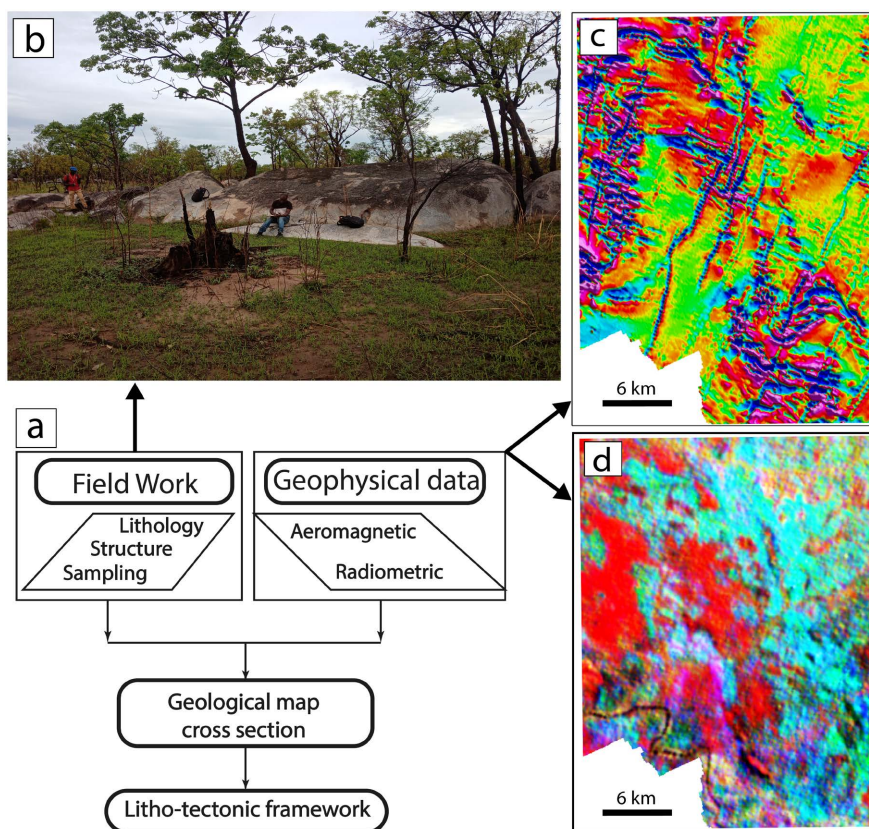
Figure 2. (a) Flow chart of investigation and data processing methodology in this study. (b) Photography of the lithological and structural data collection process during field work. (c) and (d): Airborne geophysical data. (c) magnetic map reduced to the equator and then first vertical derivative applied; (d) composite radiometric ternary map with K (red), Th (green) and U (blue) (SYSMIN, 2006).

that will be the principal base to make the litho-structural map. Structural data were reported as strike/dip/quadrant for the planar structures and plunge/azimuth for linear structures.

3.2. Aeromagnetic Data

Aeromagnetic data are a critical tool, which became essential in regional and local geology mapping and resource exploration (e.g., [14] [32] [33]). Magnetic anomalies highlight the structural framework and main geological features at the surface and in depth. The data come from two main aeromagnetic surveys which were flown covering the Malian part of the KKI during SYSMIN project [34]. Their characteristics are summarized in **Table 1**.

The first vertical derivative (1VD) is used to delineate short-wavelength features [13]. Thus, the 1VD map was used to derive the structural framework of the Dialafara area as it gives a sharper picture of the near-surface litho-structural features.

The absolute value of the analytic signal (AS) resolves close-spaced bodies' relationship and is effective for delineating geological boundaries [35].
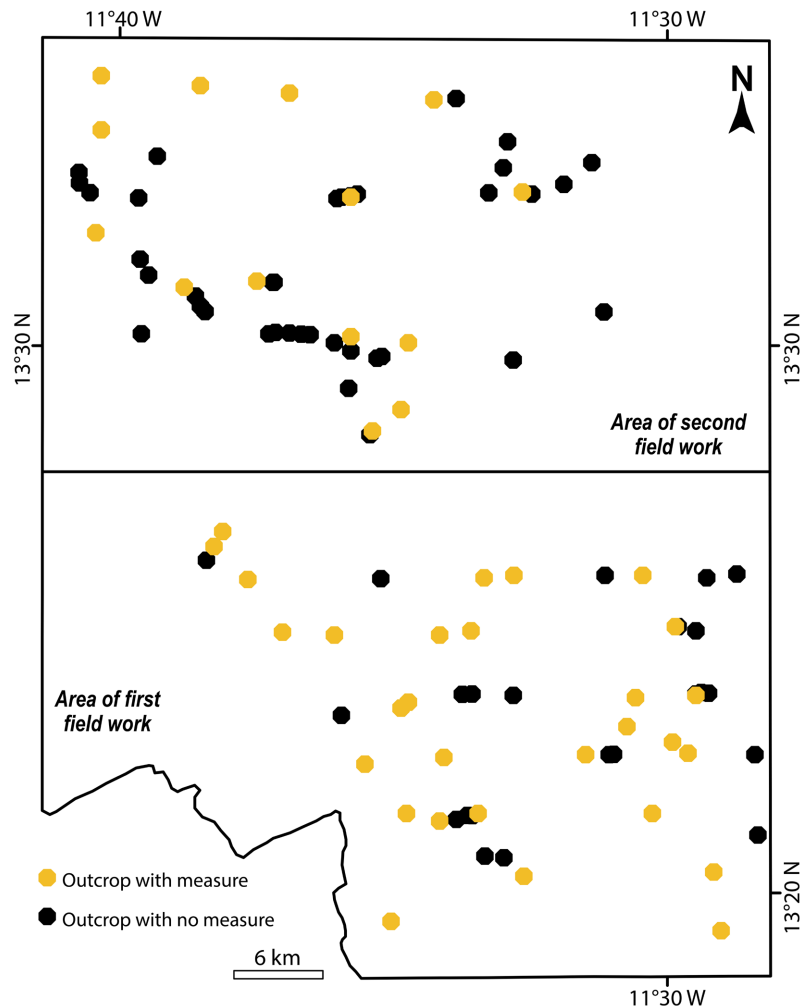
Figure 3. Outcrop map of the study area. Some points (black) indicate field-observations giving detailed lithological and structural description. Other points (yellow) present field-observations with lithological and structural description and structural measurements.

Table 1. Key parameters of geophysical data sets from Mali.

	High-Sense	Kevron
Survey area	Kéniéba	Kéniéba
Survey period	1996 and 1997	2001
Acquisition company	High-Sense Geophysics Ltd.	Kevron Pty Ltd.
Survey type	Combined airborne	Combined airborne
Altitude	100 m	100 m
Flight orientation	000˚ - 180˚ and 065˚ - 245˚	000˚ - 180˚ and 065˚ - 245˚
Line spacing	200 m	200 m
Tie line orientation	065˚ - 245˚ and 155˚ - 335˚	065˚ - 245˚ and 155˚ - 335˚
Tie line spacing	3000 m	3000 m
Time interval in recording	0.1 s	0.1 s

4. Results

4.1. Key Lithologies

This section presents the different lithology described during field work. The Dialafara area straddles the border between the Dialé-Daléma and Kofi metasedimentary units (Figure 1). However, the study area is mostly covered by a lateritic cuirass resulting from the alteration of underlying formations. All lithologies are metamorphosed to greenschist facies [28].

4.1.1. Volcanic and Volcano-Sedimentary Rocks

Volcanic rocks are formed by the solidification of fragments projected at high temperature by a volcanic eruption. The pyroclastic rocks are marked by tufs and pyroclastic flows (Figure 4). Tufs are greenish-gray rocks with dark minerals and appear as bedded and deformed bands (Figure 4(a)). Pyroclastic flows
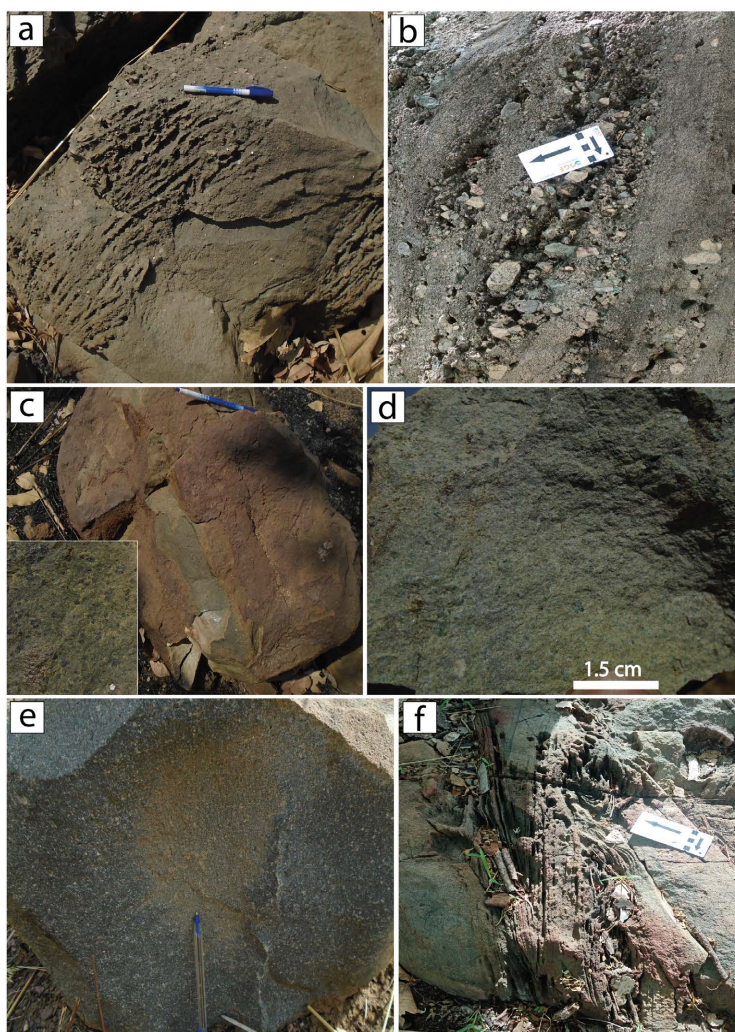

Figure 4. Field photographs of representative volcanic and volcano-sedimentary lithologies: (a) Volcanic tuff with fragments. (b) Pyroclastic rocks with angular to sub-rounded lithic fragments. (c) Basalt with crystal of black pyroxene. (d) Andesitic basalt. (e) Andesite. (f) Volcanosediment cross-cut by S_{2a} and S_{2b} schistosity.

have been mapped in the metavolcanic suite and form sporadic units with flattened bombs and angular to sub-rounded lithic fragments ranging in size from 1 to 10 cm (Figure 4(b)).

Volcanic rocks are also represented by basalt and/or basaltic andesite. These rocks have been mapped in the north-western and the south-eastern part of the study area and described as sub-units of the metavolcanic suites of the Mako belt. Basalts (Figure 4(c)) are characterized by sporadic outcrops as intercalations within volcanic suite, and are cut in places by gabbro or andesite. Basaltic andesites have been mapped in several locations (Figure 4(d)). They are characterized by a microlithic texture and a greenish color and are associated with andesites and pyroclastic flows. Andesites are characterized by slight lamination with a microlithic porphyry texture and highly variable plagioclase phenocrystal sizes (Figure 4(e)).

Volcano-sedimentary rocks are sedimentary units that originate from reworked volcanic material and/or volcanic material, which are mapped in several locations in the study area (Figure 4(f)). They consist of flysch-like metasediments, and epiclastic volcano-sediments intercalated within the matavolcanic suite.

4.1.2. Metasedimentary Rocks

The metasedimentary rocks consist of turbidite sequences metamorphosed to greenschist facies, schists and conglomerate. The turbidite sequences consist of metagreywacke intercalated with meta-argillite (Figure 5(a), Figure 5(b)). They show a very extensive surface of alteration profile and are located in the center of the sector and also slightly to the east. They form a band oriented NNE-SSW. Tectonically, the metasediments are affected by intense foliation and are usually traversed by shear zones (Figure 5(a), Figure 5(b)). Sometimes, metagreywacke is very fine, aphanitic black rock that may be meta-quartzite corresponding to tourmaline-bearing quartz-wacke, which are crosscut by quartz or quartz-carbonate veins and fractures (Figure 5(c)).

The schists make up the bulk of the lithologies encountered in the field. The schists are well straightened and finely laminated volcano-sedimentary to metasedimentary units with an NNE-SSW trending schistosity (Figure 5(d), Figure 5(e)). These schists are mauve-greyish, but can be brownish in places. The mineralogy of the schists shows a fine lepidoblastic texture with small to medium-sized grains. These grains are mainly represented by quartz, sericite, calcite and chlorite. The schists, in some cases, are intersected by quartz veins.

Conglomerates occur in massive blocks. They consist of epiclastic lithic debris (of volcanic origin), locally carbonated (Figure 5(f)). The conglomerate elements are often subjoined and highly heterometric (centimetric to decimetric). The typology of the elements reveals a great diversity of sources (Figure 5(f)). They contain pebbles of andesitic volcanics, diorites, granites, sandstones, carbonates and probably dacite and rhyolite.
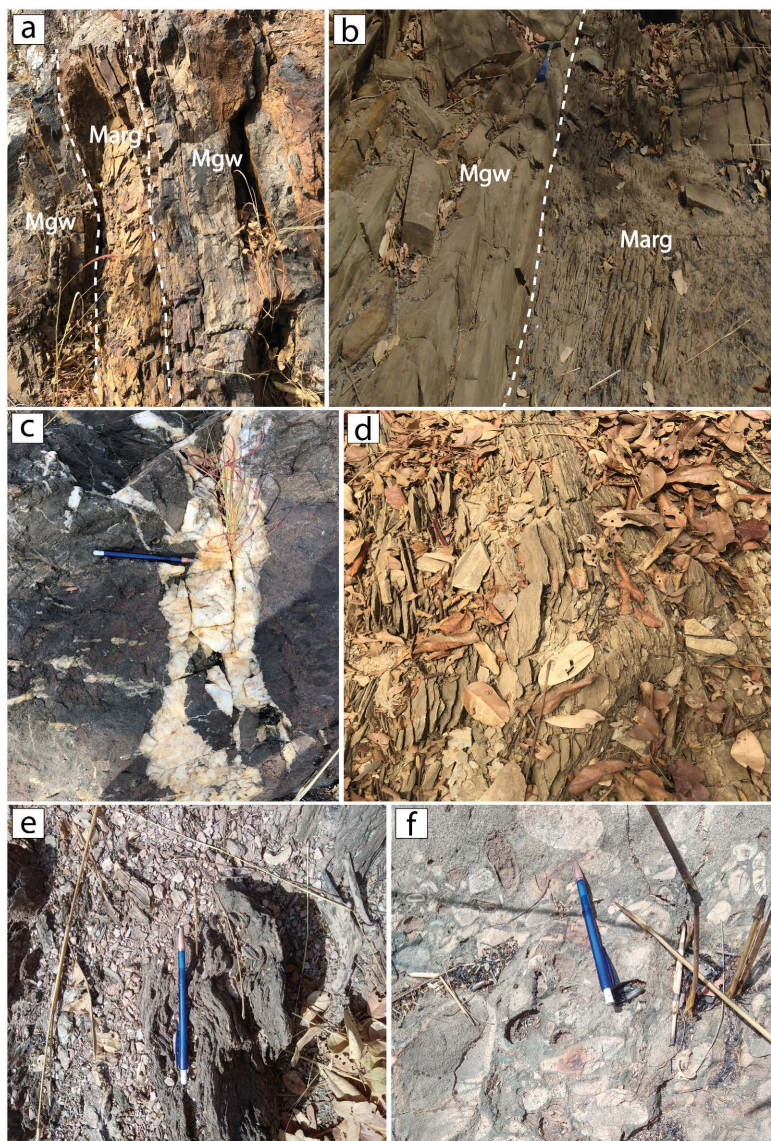
Figure 5. Field photographs of representative metasedimentary units. (a) and (b) show a turbidite sequences consisting of metagreywacke intercalated with meta-argillite. (c) Tourmaline-bearing quartz-wacke cross-cut by quart-carbonate veins. (d) and (e) show schist finely straightened by deformation. (f) Conglomerate epiclastic lithic debris of volcanic origin.

4.1.3. Plutonic Magmatic Rocks

Plutonic magmatic rocks are represented by gabbro/micro-gabbro and granodiorite/diorite. Gabbros occur as sporadic elliptical bodies or dykes (**Figure 6(a)**). They appear folded in the undifferentiated volcano-sediments units. They have a grainy texture with minerals of plagioclase, pyroxene, amphibole and little biotite (**Figure 6(b)**). They are locally composed of plagioclase megacrysts.

The granodioritic to dioritic rocks (**Figure 6(c)**) stand out in the north-eastern part of the study area, where it is mapped in a circular shape with a NW-SE trending. They are characterized by very little deformation, with local shear bands and/or mylonitic foliations (**Figure 6(d)**). Mineralogy is mainly composed of
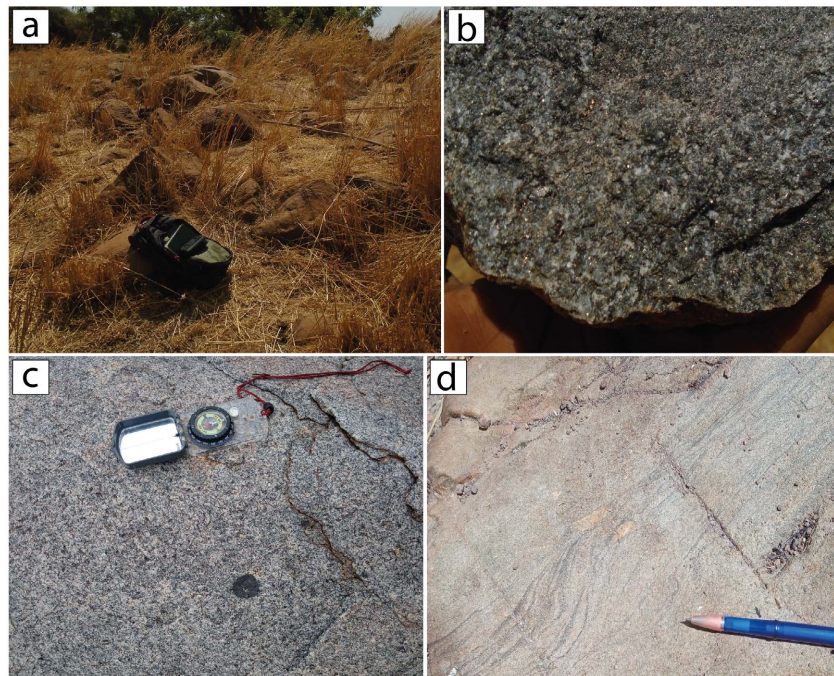
Figure 6. Field photographs of representative plutonic magmatic units. (a) and (b) Gabbro. (c) Granodiorite. (d) Diorite affected S_{2a} schistosity.

quartz, plagioclase and biotite. They are coarse-grained and sometimes porphyritic.

4.2. Structural Framework

The methodology for structural analysis includes interpretations of individual structural measurements during field work and structural interpretation of aeromagnetic data (**Figure 7** and **Table 2**). Structural measurements include schistosity, foliation, and information related to folds, faults and shear zones.

4.2.1. Ductile Deformation Phase

The earliest structural fabric is recognized in the north-western part of the Dialafara area and is appeared as a bedding-parallel S_1 schistosity (**Figure 7** and **Figure 8**). These S_1 schistosities are oriented N90° to N130° with an average dip of 50°, which are generally inclined towards the south to southwest but locally to the northeast (**Figure 7(a)**). The S_1 are associated with a NW-SE striking tight to isoclinal shear folds (F_1) with an NW-SE axial planar and point to a dominant vergence to the SE (**Figure 9**). These earliest structural fabrics are manifested in the metavolcano-plutonic Mako belt. Fold geometry and S_1 schistosities data marked the first deformation event (D_{D1}), which is consistent with a N-S directed shortening.

The first structural features of the D_{D1} are crosscut by a pervasive NNW to NE-trending structural corridors providing the foundation for formation of map-scale faults and shear zones (**Figure 9**). These structural corridors are associated to a penetrative NNW to NE-striking schistosity defined as S_2. The S_2
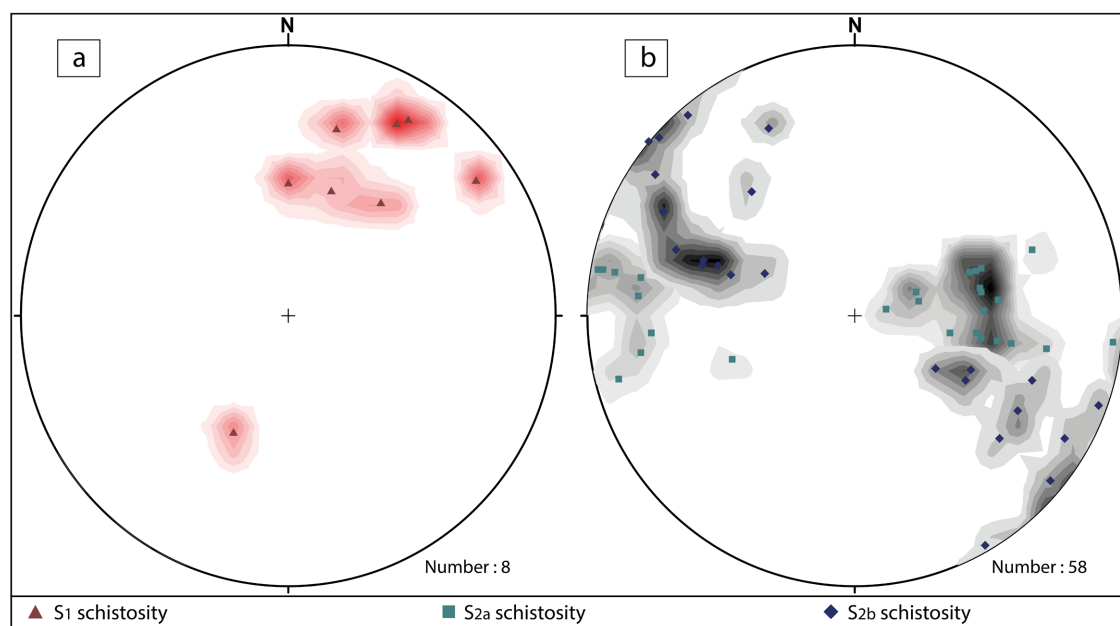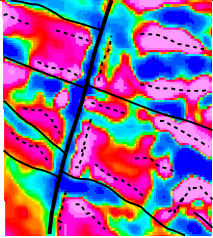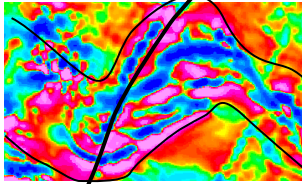
Figure 7. Equal area, lower hemisphere projections showing the orientation of the ductile deformation event in the Dialafara area. (a) shows S1 schistosity of D_{D1} deformation event. (b) shows S2a and S2b schistosity of D_{D2} deformation event.

Table 2. Zoom on near-surface deformation event interpreted in the local-scale Dialafara area and their magnetic response.

Structure	Event	Sense	Magnetic characteristic	Corresponding images
Near-surface structural framework from the first vertical derivative map	D_{D1} shear zone	WNW to NW trending	Abrupt magnetic contact between contrasting magnetic domains	
	D_{D2} shear zone	Sinistral		
	Schistosity	WNW to NW trending and NNE trending	Trend of magnetic units	
	Fold		Folded magnetic horizons with fault/shear in axial plane	
	Axial plane	NE trending		
	DD3 fault	Dextral	Straight discontinuity that cross-cut and offset magnetic units	
		NE trending		

schistosities display a variety of orientations. Some schistosities strike from N340˚ to N10˚ with an average dip of 45˚ generally inclined towards the west (S$_{2a}$) (**Figure 7(b)**). Others schistosities strike from N20˚ to N50˚ with an average dip of 70˚ inclined to both southeast and northwest (S$_{2b}$) (**Figure 7(b)**). The
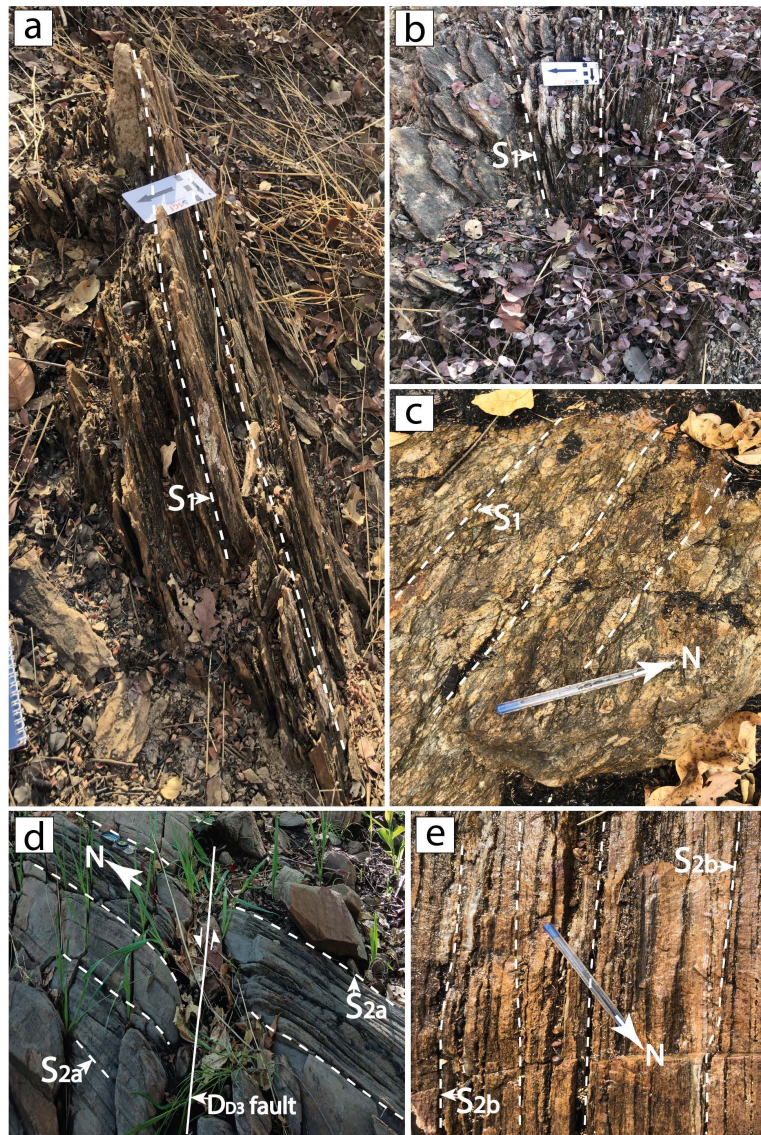
Figure 8. Field photographs of representative structures: (a) and (b) Finely flattened of metasediment units portraying S_1 schistosity. (c) Deformed conglomerate showing S_1 schistosity. (d) Deformed volcano-sedimentary unit showing S_{2a} schistosity, which is cross-cut by D_{D3} fault. (e) Deformed metagreywacke showing S_{2b} schistosity.

S_{2b} fabrics are subparallel to the axial planar of the NE-SW-striking upright to tight F_2 fold. The F_2 fold appears in the south-eastern part of the Dialafara area, which exhibits a mean axial planar striking of N42° (**Figure 9**). These structural features define the second deformation event (D_{D2}) with an E-W shortening accommodated by a horizontal stretching and a dominant simple shear component.

4.2.2. Ductile-Brittle to Brittle Deformation Phase

A set of penetrative schistosity (S_3) oriented NW-SE and NE-SW are portrayed in the Dialafara area, which are associated with a set of subvertical NW-SE and NE-SW trending ductile-brittle to brittle faults (**Figure 9** and **Table 2**). These
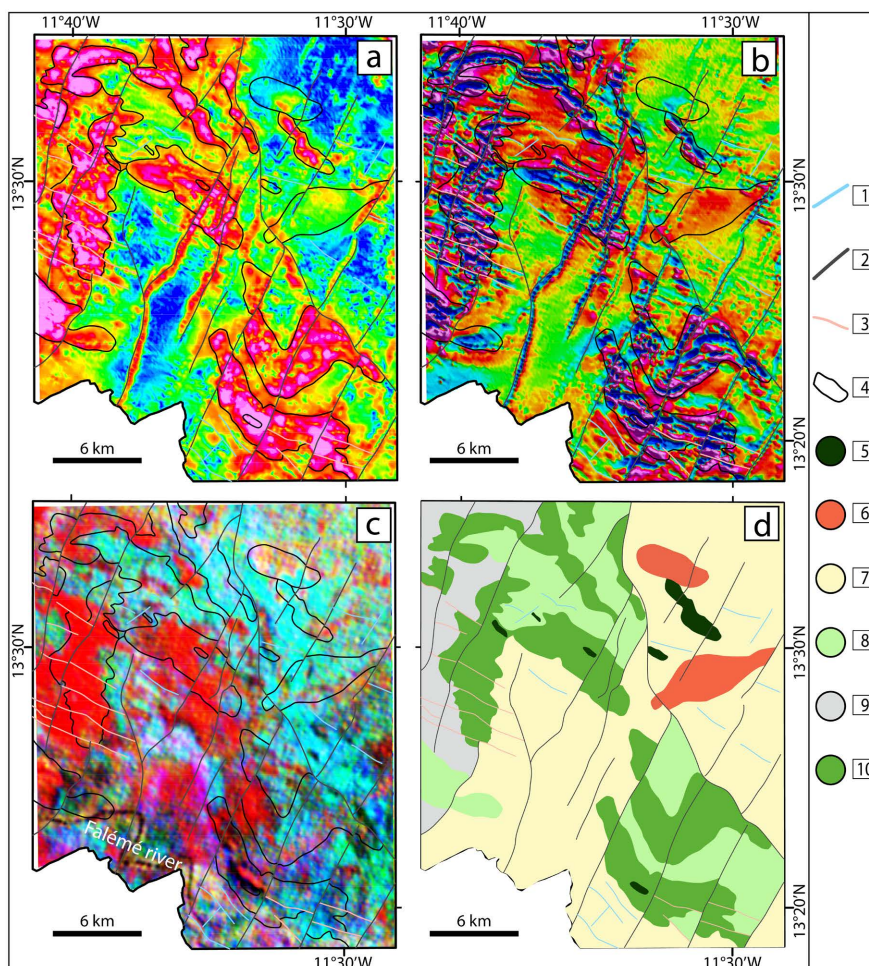
Figure 9. (a) Analytic signal of the TMI overlain by interpreted litho-structural frame. (b) First vertical derivative of the TMI overlain by interpreted litho-structural frame. (c) composite radiometric ternary map overlain by interpreted litho-structural frame. (d) Litho-structural map of the Dialafara area. 1: D_{D3} Faults; 2: D_{D2} fault/shear zones; 3: D_{D1} fault/shear zones; 4: Lithological outline; 5: Gabbro dykes; 6: Granodiorite/diorite intrusions; 7: Metasedimentary units; 8: Volcano-sedimentary units and schists; 9: Pyroclastic and tuff rocks; 10: Basalt, basaltic andesite, and andesite.

faults are up to 0.5 m wide and occur as conjugate sets. Ubiquitous ENE-WSW to E-W striking brittle fault and/or fracture were also recorded during mapping. These features can be linked to a single deformation event defined here as D_{D3}. The geometrical relationship between the different structures of the D_{D3} is consistent with E-W-directed shortening.

Milky white quartz and/or quartz-carbonate veins are commonly developed during D_{D3} and occur in almost all lithologies. They are oriented in the direction of the fractures they cover (**Figure 5(c)**).

4.3. Litho-Structural Map

The integration of geophysical and field data permits to construct a new litho-structural map of the Dialafara area (**Figure 9**). The figure shows an exam-

ple of litho-structural map based on field work and geophysical analysis and illustrates architecture of lithologies accounted in the region as well as the structural framework. The Dialafara litho-structural map shows three main parts.

- The first one is defined by volvanic and volcano-sedimentary rocks located in the north-western part (**Figure 9**). This part is characterized by heterogeneous magnetic signatures with elongate high and medium anomalies in the analytic signal as well as the first vertical derivative images (**Figure 9(a)**, **Figure 9(b)**). The high magnetic anomalies in this part are correlated with the basalt, basaltic andesite and andesite rocks. These lithologies are intruded by localized dyke of gabbro. The SE vergence fold of the moderately magnetic body in the center of this part is defined as volcano-sedimentary units (**Figure 9**). In this part, the concentration of Th and U are extremely low, as it exhibits a red color of K (**Figure 9(c)**).

- The second part is located in the south-eastern part (**Figure 9**). The area is characterized by the high anomaly values in the analytic signal and the first vertical derivative images, and is consist of metavolcanic formations dominated by volcano-sedimentary units, pyroclastics and tuffs, and schists. Gabbro dyke is defined in one place into this part. This part shows similar magnetization as the first one, although its intensity and texture are variable (**Figure 9(a)**, **Figure 9(b)**). This part shows differences about the concentration of the ratio of K, Th and U. It increases in Th and U concentration when moving into the extreme south-east (**Figure 9(c)**).

- The third part is marked by metasedimentary units and located in the south-western and the north-eastern part of the maps (**Figure 9**). In aeromagnetic data, this part is less magnetized than the two first part (**Figure 9(a)**, **Figure 9(b)**). It is mark by a smooth magnetic texture with low magnetic response. This part is intruded by granodioritic to dioritic body which is expressed by a low magnetic anomaly in the analytic signal map and by an intermediate magnetic anomaly value in the first vertical derivative map with a smooth texture (**Figure 9(a)**, **Figure 9(b)**). This part shows higher concentration of U and Th, although in the south-western side, the K content is important (**Figure 9(c)**). This is probably due to the influence of drainage of the granitoid alteration products by the Falémé river.

5. Discussion

The combination of field work and geophysical data presented in this paper provide new constraints on the lithological units and structures at the Dialafara scale (**Figure 9(d)**). The integration of geophysical data interpretation, especially the magnetic data, with structural field reconnaissance led to several findings in the Dialafara area.

The previous litho-tectonic map of the KKI presents the Dialafara area as composed by volcanoclastic rocks and metasediments (**Figure 1(b)**). This study shows that in the Dialafara area, the lithology is diverse and composed by vol-

canic and volcano-sedimentary rocks, metasedimentary units as well as plutonic intrusion (Figure 9(d)). This complexity of lithology can be distinguishing in aeromagnetic map, leading to areas on the map with different magnetization and texture.

Combined with the structural measurements, the aeromagnetic data provide sufficiently the structural framework in the Dialafara areas, where outcrop conditions are very limited (Figure 9, Table 2). This structural framework is defined by three phases of deformation (D_{D1} to D_{D3}) under ductile to brittle event. The first phase is associated with a NW-SE striking tight to isoclinal shear folds (F_1) with an NW-SE axial planar and a dominant vergence to the SE. The second phase is marked by a pervasive NNW to NE-trending structural corridors portraying map-scale faults and shear zones of the Dialafara area as well as the upright to tight F_2 fold. The previous structures are crosscut by a set NW-SE and NE-SW trending ductile-brittle to brittle faults, defining the third phase of deformation in the Dialafara area. Although, the dominant structural context was
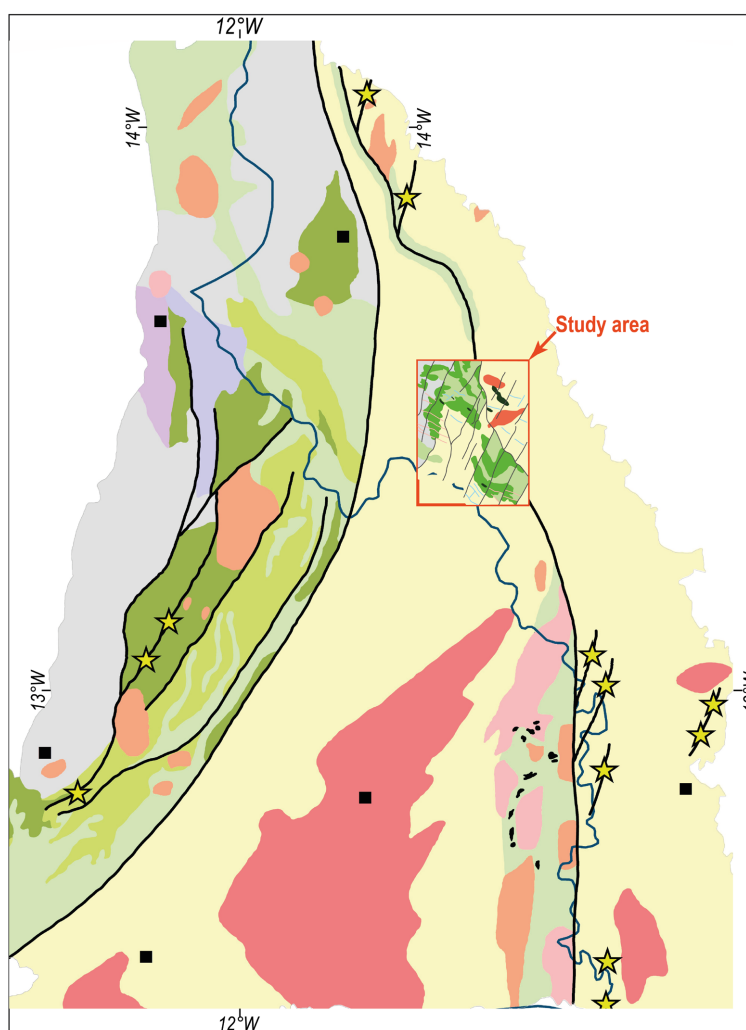

Figure 10. Integration of the Dialafara area with regional geology and tectonics into the Kédougou-Kéniéba Inlier framework.

mostly portrayed during the D_{D2} deformation event. The structural complex of this area can be a potential target for mineral exploration as it is located between the Sadiola deposit district in the north and the Loulo deposit district in the south (Figure 1(b) and Figure 10).

This study provides an important detail concerning the litho-structural context of Dialafara, showing the lithological and structural complexity of a zone that appeared monotonous in previous studies (Figure 10). This shows that the Falémé belt probably continues as far as the Mako belt, and that the Falémé belt separates the two sedimentary series of Dialé-Daléma to the south-west and Kofi to the east.

6. Conclusions

This study shows that the combination of field reconnaissance and magnetic data interpretation, leads to several discoveries. This work complements previously published work enabling to portray a new litho-tectonic map of the Dialafara area (Figure 9(d)).

Field work has shown that the Dialafara area is a complex lithological zone. This was confirmed by aeromagnetic data as it is characterized by heterogeneous magnetic signatures with high to low anomalies. The magnetic grain in the aeromagnetic data combined with structural measurements in the field is interpreted to reflect deformed magnetic horizons. This combination permits to portray a complex structural framework of the study area with three deformation phases (D_{D1} to D_{D3}). The metallogenic nature and significance of these structures have not been identified, but they should be a potential target for mineral prospective as these structures could be a continuity of mineralized structures from Loulo to Sadiola gold districts.

Acknowledgements

Conflicts of Interest

The authors declare no conflicts of interest regarding the publication of this paper.

References

[1] Goldfarb, R.J., André-Mayer, A.S., Jowitt, S.M. and Mudd, G.M. (2017) West Africa: The World's Premier Paleoproterozoic Gold Province. *Economic Geology*, **112**,

123-143. https://doi.org/10.2113/econgeo.112.1.123

[2] Bonhomme, M. (1962) Contribution à l'étude géochronologique de la plate-forme de l'Ouest africain. Imprimerie Louis-Jean, Québec.

[3] Milési, J.P., Ledru, P., Feybesse, J.L., Dommanget, A. and Marcoux, E. (1992) Early Proterozoic Ore Deposits and Tectonics of the Birimian Orogenic Belt, West Africa. *Precambrian Research*, **58**, 305-344. https://doi.org/10.1016/0301-9268(92)90123-6

[4] Liégeois, J.P., Claessens, W., Camara, D. and Klerkx, J. (1991) Short-Lived Eburnian Orogeny in Southern Mali. Geology, Tectonics, U-Pb and Rb-Sr Geochronology. *Precambrian Research*, **50**, 111-136. https://doi.org/10.1016/0301-9268(91)90050-K

[5] Feybesse, J.L., Billa, M., Guerrot, C., Duguey, E., Lescuyer, J.L., Milesi, J.P. and Bouchot, V. (2006) The Paleoproterozoic Ghanaian Province: Geodynamic Model and Ore Controls, Including Regional Stress Modeling. *Precambrian Research*, **149**, 149-196. https://doi.org/10.1016/j.precamres.2006.06.003

[6] Vanderhaeghe, O. and Teyssier, C. (2001) Partial Melting and Flow of Orogens. *Tectonophysics*, **342**, 451-472. https://doi.org/10.1016/S0040-1951(01)00175-5

[7] Choukroune, P., Ludden, J.N., Chardon, D., Calvert, A.J. and Bouhallier, H. (1997) Archaean Crustal Growth and Tectonic Processes: A Comparison of the Superior Province, Canada and the Dharwar Craton, India. *Geological Society Special Publications*, **121**, 63-98. https://doi.org/10.1144/GSL.SP.1997.121.01.04

[8] Gueye, M., Ngom, P.M., Diène, M., Thiam, Y., Siegesmund, S., Wemmer, K. and Pawlig, S. (2008) Intrusive Rocks and Tectono-Metamorphic Evolution of the Mako Paleoproterozoic Belt (Eastern Senegal, West Africa). *Journal of African Earth Sciences*, **50**, 88-110. https://doi.org/10.1016/j.jafrearsci.2007.09.013

[9] Goldfarb, R.J., Phillips, G.N. and Nokleberg, W.J. (1998) Tectonic Setting of Syn-Orogenic Gold Deposits of the Pacific Rim. *Ore Geology Reviews*, **13**, 185-218. https://doi.org/10.1016/S0169-1368(97)00018-8

[10] Groves, D.I., Santosh, M., Goldfarb, R.J. and Zhang, L. (2018) Structural Geometry of Orogenic Gold Deposits: Implications for Exploration of World-Class and Giant Deposits. *Geoscience Frontiers*, **9**, 1163-1177. https://doi.org/10.1016/j.gsf.2018.01.006

[11] Kusnir, I. (1991) Gold in Mali. *Acta Montanistica Slovaca*, **4**, 311-318.

[12] Milési, J.P., Heinry, C. and Sylvain, J.P. (1989) Minéralisations aurifères de l'Afrique de l'ouest leurs relations avec l'évolution lithostructurale au Proterozoique inférieur. Bureau de recherches géologiques et minières, Orléans.

[13] Gunn, P.J., Maidment, D. and Milligan, P.R. (1997) Interpreting Aeromagnetic Data in Areas of Limited Outcrop. *AGSO Journal of Australian Geology & Geophysics*, **17**, 175-185.

[14] Hansen, R.O. (2001) Gravity and Magnetic Methods at the Turn of the Millennium. *Geophysics*, **66**, 36-37. https://doi.org/10.1190/1.1444915

[15] Metelka, V., Baratoux, L., Jessell, M.W., Barth, A., Ježek, J. and Naba, S. (2018) Automated Regolith Landform Mapping Using Airborne Geophysics and Remote Sensing Data, Burkina Faso, West Africa. *Remote Sensing of Environment*, **204**, 964-978. https://doi.org/10.1016/j.rse.2017.08.004

[16] Pereira, L.C.L., De Lira Santos, L.C.M. and Carrino, T.A. (2019) The Role of Airborne Geophysics in the Investigation of Gold Occurrences in the Itapetim Region, Borborema Province, Northeast Brazil. *Brazilian Journal of Geology*, **49**, e20190028. https://doi.org/10.1590/2317-4889201920190028

[17] Hirdes, W. and Davis, D.W. (2002) U–Pb Geochronology of Paleoproterozoic

Rocks in the Southern Part of the Kedougou-Kenieba Inlier, Senegal, West Africa: Evidence for Diachronous Accretionary Development of the Eburnean Province. *Precambrian Research*, **118**, 83-99. https://doi.org/10.1016/S0301-9268(02)00080-3

[18] Dia, A., Van Schmus, W.R. and Kröner, A. (1997) Isotopic Constraints on the Age and Formation of a Palaeoproterozoic Volcanic Arc Complex in the Kédougou Inlier, Eastern SENEGAL, West Africa. *Journal of African Earth Sciences*, **24**, 197-213. https://doi.org/10.1016/S0899-5362(97)00038-9

[19] Dioh, E., Béziat, D., Debat, P., Grégoire, M. and Ngom, P.M. (2006) Diversity of the Palaeoproterozoic Granitoids of the Kédougou Inlier (Eastern Senegal): Petrographical and Geochemical Constraints. *Journal of African Earth Sciences*, **44**, 351-371. https://doi.org/10.1016/j.jafrearsci.2005.11.024

[20] Bassot, J.P. (1987) Le complexe volcano-plutonique calco-alcali de la riviere dalema (Est Senegal): Discussion de sa signification geodynamique dans le cadre de l'orogenie eburneenne (proterozoique inferieur). *Journal of African Earth Sciences* (1983), **6**, 505-519. https://doi.org/10.1016/0899-5362(87)90091-1

[21] Schwartz, M.O. and Melcher, F. (2004) The Falémé iron district, Senegal. *Economic Geology*, **99**, 917-939. https://doi.org/10.2113/gsecongeo.99.5.917

[22] Lambert-Smith, J.S., Lawrence, D.M., Vargas, C.A., Boyce, A.J., Treloar, P.J. and Herbert, S. (2016) The Gounkoto Au deposit, West Africa: Constraints on Ore Genesis and Volatile Sources from Petrological, Fluid Inclusion and Stable Isotope Data. *Ore Geology Reviews*, **78**, 606-622. https://doi.org/10.1016/j.oregeorev.2015.10.025

[23] Bassot, J.P. (1966) Étude géologique du Sénégal oriental et de ses confins guinéo-maliens... Éditions BRGM, Paris.

[24] Koné, J., Vanderhaeghe, O., Diatta, F., Baratoux, L., Thébaud, N., Bruiguier, O., Ndiaye, P.M., Duchene, S., Pitra, P. and Ganne, J. (2020) Source and Deposition Age of the Dialé-Daléma Metasedimetary Series (Kédougou-Kénieba Inlier, Senegal) Constrained by U-Pb Geochronology on Detrital Zircons. *Journal of African Earth Sciences*, **165**, Article ID: 103801. https://doi.org/10.1016/j.jafrearsci.2020.103801

[25] Pons, J., Oudin, C. and Valero, J. (1992) Kinematics of Large Syn-Orogenic Intrusions: Example of the Lower Proterozoic Saraya Batholith (Eastern Senegal). *Geologische Rundschau*, **81**, 473-486. https://doi.org/10.1007/BF01828610

[26] Masurel, Q., Thébaud, N., Miller, J. and Ulrich, S. (2017) The Tectono-Magmatic Framework to Gold Mineralisation in the Sadiola-Yatela Gold Camp and Implications for the Paleotectonic Setting of the Kédougou-Kénieba Inlier, West Africa. *Precambrian Research*, **292**, 35-56. https://doi.org/10.1016/j.precamres.2017.01.017

[27] Allibone, A., Lawrence, D., Scott, J., Fanning, M., Lambert-Smith, J., Stenhouse P., Harbidge, R., Vargas, C., Rose Turnbull, R. and Holliday, J. (2020) Early Paleoproterozoic Gold Deposits of the Loulo District, Western Mali. In: Sillitoe, R.H., Goldfarb, R.J., Robert, F. and Simmons, S.F., Eds., *Geology of the World's Major Gold Deposits and Provinces*, Society of Economic Geologists, Littleton, 141-162. https://doi.org/10.5382/SP.23.07

[28] Ledru, P., Pons, J., Milési, J.P., Feybesse, J.L. and Johan, V. (1991) Transcurrent Tectonics and Polycyclic Evolution in the Lower Proterozoic of Senegal-Mali. *Precambrian Research*, **50**, 337-354. https://doi.org/10.1016/0301-9268(91)90028-9

[29] Diene, M., Gueye, M., Diallo, D.P. and Dia, A. (2012) Structural Evolution of a Precambrian Segment: Example of the Paleoproterozoic Formations of the Mako Belt (Eastern Senegal, West Africa). *International Journal of Geosciences*, **3**, 153-165.

https://doi.org/10.4236/ijg.2012.31017

[30] Diallo, M., Lenka, B., Dufréchou, G., Jessel, M.W., Vanderhaeghe, O., Ly, S. and Baratoux, D. (2020) Structure of the Paleoproterozoic Kédougou-Kéniéba Inlier (Senegal-Mali) Deduced from Gravity and Aeoromagnetic Data. *Journal of African Earth Sciences*, **162**, Article ID: 103732.
https://doi.org/10.1016/j.jafrearsci.2019.103732

[31] Bassot, J.P. and Dommanget, A. (1986) Mise en évidence d'un accident majeur affectant le Protérozoïque inférieur des confins sénégalo-maliens. *Comptes rendus hebdomadaires des séances de l'Académie des sciences*, **302**, 1101-1106.

[32] Boyd, D.M. and Isles, D.J. (2007) Geological Interpretation of Airborne Magnetic Surveys-40 Years on. *Proceedings of Exploration* 07: *Fifth Decennial International Conference on Mineral Exploration*, Toronto, 9-12 September 2007, 491-505.

[33] Koné, A.Y., Nasr, I.H., Traoré, B., Amiri, A., Inoubli, M.H., Sangaré, S. and Qaysi, S. (2021) Geophysical Contributions to Gold Exploration in Western Mali according to Airborne Electromagnetic Data Interpretations. *Minerals*, **11**, Article 126.
https://doi.org/10.3390/min11020126

[34] Sysmin (2006) Projet de cartographie du Birimien malien. BRGM/RC-54684-FR.

[35] McLeod, I.N., Jones, K. and Dai, T.F. (1993) 3-D Analytic Signal in the Interpretation of Total Magnetic Field Data at Low Magnetic Latitudes. *Exploration Geophysics*, **24**, 679-687. https://doi.org/10.1071/EG993679